ELSEVIER

Contents lists available at ScienceDirect

Computer Physics Communications

www.elsevier.com/locate/cpc



IrRep: Symmetry eigenvalues and irreducible representations of *ab initio* band structures $^{,, , , , , }$



Mikel Iraola a,b, Juan L. Mañes b, Barry Bradlyn c, Matthew K. Horton d,e, Titus Neupert d,b, Maia G. Vergniory d,g,*, Stepan S. Tsirkin d,b

- ^a Donostia International Physics Center, 20018 Donostia-San Sebastian, Spain
- b Department of Condensed Matter Physics, University of the Basque Country UPV/EHU, Apartado 644, 48080 Bilbao, Spain
- ^c Department of Physics and Institute of Condensed Matter Theory, University of Illinois at Urbana-Champaign, IL 61801, USA
- d Energy Technologies Area, Lawrence Berkeley National Laboratory, Berkeley, USA
- ^e Materials Science and Engineering, University of California, Berkeley, USA
- f Department of Physics, University of Zurich, Winterthurerstrasse 190, CH-8057 Zurich, Switzerland
- g IKERBASQUE, Basque Foundation for Science, Maria Diaz de Haro 3, 48013 Bilbao, Spain

ARTICLE INFO

Article history: Received 13 January 2021 Received in revised form 26 October 2021 Accepted 3 November 2021 Available online 16 November 2021

Keywords:
DFT
Symmetry
Irreducible representations
Topology
Python
Bandstructure

ABSTRACT

We present IrRep – a Python code that calculates the symmetry eigenvalues of electronic Bloch states in crystalline solids and the irreducible representations under which they transform. As input it receives bandstructures computed with state-of-the-art Density Functional Theory codes such as VASP, Quantum Espresso, or Abinit, as well as any other code that has an interface to Wannier90. Our code is applicable to materials in any of the 230 space groups and double groups preserving time-reversal symmetry with or without spin-orbit coupling included, for primitive or conventional unit cells. This makes IrRep a powerful tool to systematically analyze the connectivity and topological classification of bands, as well as to detect insulators with non-trivial topology, following the Topological Quantum Chemistry formalism: IrRep can generate the input files needed to calculate the (physical) elementary band representations and the symmetry-based indicators using the *CheckTopologicalMat* routine of the Bilbao Crystallographic Server. It is also particularly suitable for interfaces with other plane-waves based codes, due to its flexible structure.

Program summary

Program Title: IrRep

CPC Library link to program files:: https://doi.org/10.17632/yznd2ky9r6.1 Developer's repository link: https://github.com/stepan-tsirkin/irrep

Licensing provisions: GPLv3 Programming language: Python

Nature of problem: Symmetry properties of electronic band structures in solids are tightly related to their topological features. This relation is set mathematically by the formalisms of Topological Quantum Chemistry [1,2] and symmetry-based indicators of topology [3], but their application requires knowledge of the irreducible representations of the bands. Therefore, a code to calculate irreducible representations of ab initio bands is essential for a systematic theoretical search and classification of topological materials. Solution method: Irrepresentations from files generated by VASP, Abinit, or Quantum Espresso (also files written as input for Wannier90), determines the space group and symmetry operations via the spglib library, evaluates the eigenvalues of the symmetry operations for the selected bands, and applies Group Theory to determine their irreducible representations.

References

[1] Barry Bradlyn, L. Elcoro, Jennifer Cano, M. G. Vergniory, Zhijun Wang, C. Felser, M. I. Aroyo, and B. Andrei Bernevig, Nature 547, 298-305 (2017).

E-mail addresses: mikel.i.iraola@gmail.com (M. Iraola), maiagvergniory@dipc.org (M.G. Vergniory).

The review of this paper was arranged by Prof. David W. Walker.

^{††} This paper and its associated computer program are available via the Computer Physics Communications homepage on ScienceDirect (http://www.sciencedirect.com/science/journal/00104655).

^{*} Corresponding author.

- [2] M. G. Vergniory, L. Elcoro, C. Felser, N. Regnault, B. A. Bernevig, and Z. Wang, Nature 566, A complete catalogue of high-quality topological materials, Nature 566, 480-485 (2019).
- [3] Hoi Chun Po, Ashvin Vishwanath, and Haruki Watanabe, Nat. Commun. 8, 50 (2017).

© 2021 Elsevier B.V. All rights reserved.

1. Introduction

Symmetries are fundamental to the properties of quantum systems [1]. In particular, knowledge of the symmetry operations under which energy eigenstates transform is crucial to determine the degeneracy of energy levels, the allowed couplings to external fields, and the effect of symmetry-breaking perturbations. For instance, the degeneracies present in the vibrational spectrum of a molecule are determined by the dimensions of its symmetry group's irreducible (co-)representations (IRs). For electrons in periodic crystals, the band structure of a material in reciprocal space cannot be characterized without studying the symmetry properties of its wave functions [2,3]: symmetries can protect or prevent band crossings, predict splittings produced by spin-orbit coupling, and explain gap openings coming from specific terms in the Hamiltonian.

With the discovery of topological insulators [4,5], the symmetry analysis of band structures has regained importance. Recently it was discovered that electrons in periodic lattices with crystalline symmetries can yield rich physics due to the interplay of symmetry and topology [6–12]. Two main developments in the application of symmetry to the identification and classification of topological insulators gave a gigantic push to the field: First, the theory of Topological Quantum Chemistry (TQC) [13–15] built upon physical elementary band representations (PEBRs) classified all possible atomic limits in all nonmagnetic materials, identifying topological bands as those that cannot be expressed as a sum of band representations. Among the topological bands, a subset can be distinguished from trivial bands by computing a set of symmetry-based indicators [16–18] from the irreducible representations under which the bands transform. The set of symmetry-based indicators in each space group can be computed from the band representations, and have been tabulated in [19,20]. Calculation of the IRs of bands at high-symmetry points is fundamental for the application of these methods and has led to the prediction of many topological insulators [21–24] and new phases [25–35].

In this work we present IrRep, a robust, open source Python code that calculates symmetry eigenvalues and IRs of the wave functions at high-symmetry points in reciprocal space for any band structure computed by means of Density Functional Theory (DFT). Currently, IrRep can interface directly with 3 widely used plane-wave DFT codes: the Vienna Ab initio Simulation Package (VASP) [36], Abinit [37] and Quantum Espresso (QE) [38]. IrRep can also read input files in Wannier90 (W90) [39] format (.win, .eig, UNK), prepared by interfaces like pw2wannier90. This allows IrRep to be used with any code that has a W90 interface, such as SIESTA [40]. Furthermore, it has been structured in a user friendly format allowing the implementation of routines to interface with any other plane-wave based code.

Although similar codes exist for VASP [41] (vasp2trace, used to calculate the topological bands in [21,24,42] materials database) and QE [43], IrRep is the only code that does not restrict the user to a single DFT program. Moreover, our code follows the same notation as the popular Bilbao Crystallographic Server (BCS) [44] to identify the IRs, which avoids confusion coming from the lack of an official standard notation, especially for spin-orbit coupled systems. Tables of IRs are encapsulated within the code package, so that IrRep can determine IRs without extra input from the user. The output is written in a form that is compatible with the *CheckTopologicalMat* tool of the BCS [21]. As additional functionality, IrRep can separate bands by eigenvalues of certain symmetry operator and calculates the \mathbb{Z}_2 and \mathbb{Z}_4 topological indices of time-reversal symmetric band structures [4]. The code evolved from the routines written for Ref. [45] to determine the eigenvalues of screw rotations. At a testing level, the code was used in Refs. [28,46–49] for topological quantum chemistry analysis, and in Refs. [50,51] to analyze the dipole selection rules for optical matrix elements.

In section 2 we will introduce the basic concepts of Group Theory underlying the operation of IrRep. In section 3 we will present the workflow of the code. Finally, section 4 will be devoted to several examples, illustrating the capabilities of IrRep code for the analysis of symmetry and topology.

2. Symmetry properties of bands: irreducible representations

In this section we give a brief overview of the application of group theory to electronic Bloch states. However, only the minimal information necessary to introduce the notation and explain the functionality of the code is provided. More details may be found in classic textbooks such as [3,52].

The group G of symmetry operations that leave a crystal invariant is called the space group of the crystal. In particular, G contains all translations by vectors of the Bravais lattice. The (infinite) group of all translations is generated by 3 primitive basis vectors of the lattice, and forms the (normal) translation subgroup T of the space group G. This allows us to write the coset decomposition of G with respect to T,

$$G = T + g_1 T + g_2 T + \dots + g_N T, \tag{1}$$

where $g_1, g_2, ..., g_N$ are called the coset representatives of the decomposition. Notice that the set of coset representatives is finite and nonunique (two coset representatives differing by a translation characterize the same coset). The number N of cosets in the decomposition Eq. (1) is equal to the order of the point group $\overline{G} = G/T$ (though the set of coset representatives themselves need not be a point group for non-symmorphic lattices). Using this decomposition, any space group can be expressed in terms of the coset representatives and lattice vectors of the Bravais lattice.

The symmetries of the space group have a well-defined action on the Hilbert space of electronic states in the crystal. We denote by U_g the representation of a certain symmetry operation $g \in G$ on the Hilbert space. Since every $g \in G$ is a symmetry of the crystal, each representation matrix U_g commutes with the Hamiltonian matrix H, i.e., $[U_g, H] = 0$. Note that H is block diagonal in reciprocal space and each block $H(\mathbf{k})$ can be put in correspondence to a vector \mathbf{k} belonging to the first Brillouin zone (BZ). Although the whole matrix H

commutes with U_g , for a general $g \in G$, a block H(k) may not commute, but rather must be linearly related to H(gk), i.e. the operation g transforms k into another reciprocal vector gk. If we use Wigner-Seitz notation $g = \{R \mid v\}$ for the space group operations, then gk = Rk. The set of $g \in G$ that leave k invariant (up to a reciprocal lattice vector G) is called the little group G_k of k.

Note that the coset decomposition of Eq. (1) can also be applied to the little group G_k :

$$G_{\mathbf{k}} = T + g_1^{\mathbf{k}} T + g_2^{\mathbf{k}} T + \dots + g_M^{\mathbf{k}} T,$$
 (2)

where $M \leq N$ since $G_k \leq G$. The coset representatives g_i^k can all be chosen to be point group elements only if G_k is a symmorphic space group. For example, a group containing screw rotations or glide reflections does not contain its point group as a subgroup. In any case, the rotational parts R_i of the representatives $g_i^k = \{R_i \mid \mathbf{v}_i\}$ do form a point group \overline{G}_k , called little co-group of k. While the little group G_k is infinite, since it contains all translations, the little co-group \overline{G}_k is finite.

Consider a set $\{|\Psi_{1k}\rangle, |\Psi_{2k}\rangle, ..., |\Psi_{Dk}\rangle\}$ of eigenstates of $H(\mathbf{k})$, closed under the action of $G_{\mathbf{k}}$. When a symmetry operation $g \in G_{\mathbf{k}}$ acts on $|\Psi_{nk}\rangle$, the state undergoes a linear transformation

$$g|\Psi_{i\mathbf{k}}\rangle = \sum_{j=1}^{D} K^{ji}(g)|\Psi_{j\mathbf{k}}\rangle. \tag{3}$$

The matrices K(g) in Eq. (3) form the representation K of G_k defined in the invariant space spanned by $\{|\Psi_{nk}>\}_D$. It is said that K is an IR, if this space cannot be written as a direct sum of smaller non-trivial invariant subspaces. Every representation is characterized by the set of traces $\chi_K(g) = TrK(g)$, known as the *character* of the representation.

In general, the closed set $\{|\Psi_{nk}\rangle\}_D$ contains eigenstates transforming under more than one IR of G_k , meaning that the whole representation K is reducible and can be decomposed as a combination of these IRs

$$K = \bigoplus_{\alpha} m_{\alpha}^{\mathbf{k}} K_{\alpha}, \tag{4}$$

where K_{α} is the α^{th} IR of $G_{\mathbf{k}}$. Its multiplicity $m_{\alpha}^{\mathbf{k}}$ can be computed by means of the following expression, often referred to as the magic formula [53,54]

$$m_{\alpha}^{\mathbf{k}} = \frac{1}{\|\overline{G}_{\mathbf{k}}\|} \sum_{g \in \{g_{i}^{\mathbf{k}}\}} \chi_{K}^{*}(g) \chi_{\alpha}(g), \tag{5}$$

with $\{g_i^k\}$ denoting the set of coset representatives in the decomposition of G_k , and $\|\overline{G}_k\|$ the number of symmetry operations in the little cogroup $\overline{G}_k = G_k/T$. χ_α and χ_K indicate the characters corresponding to the IR K_α and the representation K to be decomposed, respectively. IrRep uses this formula to determine the IRs of the eigenstates of H(k) at high-symmetry points in the BZ.

3. Implementation in IrRep code

In this section, we present the workflow of the IrRep code and describe its main functionalities and the particularities of the interface to each DFT software.

3.1. Reading DFT data and input parameters

To keep the interaction with the user simple, IrRep reads as much needed information as possible from the DFT code's output files. Only parameters determining the user-defined task should be given in the command line (CLI) in the format

```
irrep -<keyword1>=<value1> -<keyword2>=<value2> ...
```

Alternatively, parameters may be set in YAML or JSON format in an input file passed to IrRep via the parameter config, as we show in the following lines:

```
irrep -config=input_filename.yml
```

Descriptions of all parameters and their default values can be found in Table 1 and they can be listed in the CLI by running IrRep's help interface:

```
irrep --help
```

Depending on the DFT code used to calculate wave functions, a different interface should be chosen to parse the corresponding DFT output files (see Table 2). The interfaces are selected with the keyword code; currently, it includes interfaces to VASP [36], Abinit [37] and QE [38]. It can also read the input files for W90 [39], which allows IrRep to be used with any of the multiple codes that support the Wannier90 interface.

While most of the keywords are self-explanatory, the meaning of the keywords refuce and shiftuce requires some elaboration. The tables of IRs are written for the conventional unit cell corresponding to the space group, i.e. the cell whose lattice vectors are parallel to the symmetry directions of the lattice. However, the DFT calculation may be done in any primitive cell. Let $\{a_1, a_2, a_3\}$ denote the

Table 1

Principal keywords to fix running options with IrRep and their function. If no value is set for parameters that are None by default, they and the functions corresponding to them will be ignored. Boolean parameters work as flags (for example, spinor is set to True by passing -spinor to the command irrep in the CLI).

Keyword	Function	Default	
code	Name of the DFT code; vasp, vasp espresso, abinit, wannier90		
fWAV	VASP input file with wave functions	WAVECAR	
fPOS	VASP input file with the crystal structure	POSCAR	
fWFK	Abinit input file with wave functions	Mandatory if code=abinit	
prefix	Variable prefix in QE calculation or seedname in W90	Mandatory if code=espresso or code=wannier90	
IBstart	First band to be considered	0, first band in DFT	
IBend	Last band to be considered	Last band in DFT calculation	
spinor	Whether wave functions are spinors or not	False (mandatory for vasp)	
Ecut	Plane wave cutoff to be applied (in eV). Usually, a value around 50 eV yields accurate results	Cutoff used for the DFT calculation	
kpoints	Indices of <i>k</i> -points at which IRs must be computed	All k-points	
kpnames	Labels of k -points at which IRs must be computed	None, not needed to calculate the traces but mandatory to assign IRs to them	
refUC	Transformation of basis vectors with respect to standard setting	Calculated automatically	
shiftUC	Shift of origin with respect to standard setting	Calculated automatically	
onlysym	Stop after finding symmetries	False	
isymsep	Index of symmetries to separate eigenstates	None	
ZAK	Calculate ZAK phases	False	
WCC	Calculate wannier charge centers	False	
plotbands	Write files for gnuplot with all symmetry eigenvalues	False	
plotFile	File where bands for plotting will be written	None	
EF	Fermi energy to shift energy levels	0.0 eV	
degenThresh	Threshold to decide whether bands are degenerate	10^{-4} eV	
groupKramers	Group wave functions in pairs of Kramers	True	
symmetries	Indices of symmetries to be printed	All symmetries	
suffix	Suffix to name files for band plotting	tognuplot	
config	Path of .yml or .json file with input parameters	None, read input parameters from CLI	

Table 2
Files read by IrRep depending on the chosen interface.

interface	-code=	files
VASP	vasp	POSCAR and WAVECAR
Abinit	abinit	*_WFK
QE	espresso	*.save/data_file_schema.xml and *.save/wfc*.dat
Wannier90	wannier90	*.win, *.eig, UNK*

basis vectors of the cell adopted for the calculation and $\{c_1, c_2, c_3\}$ those of the conventional setting, refuc is the 3 × 3 matrix M that expresses the relation between them, according to the following expression

$$(\boldsymbol{c}_1, \boldsymbol{c}_2, \boldsymbol{c}_3)^T = M(\boldsymbol{a}_1, \boldsymbol{a}_2, \boldsymbol{a}_3)^T. \tag{6}$$

Similarly, shiftUC describes the shift of the origin with respect to the origin of the conventional unit cell. Note that shiftUC and refUC are relevant only to determine the names of IRs in the notation of BCS. The characters can be computed with any choice of unit

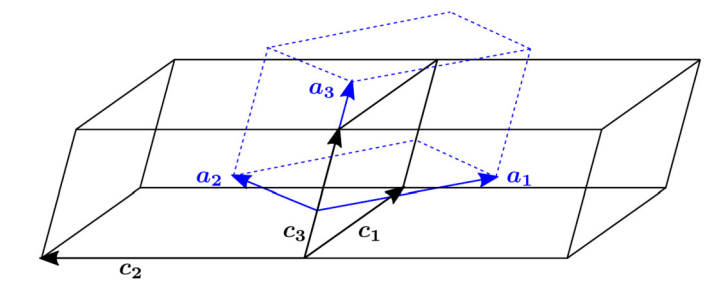


Fig. 1. The two choices considered for the unit cell of the C-centered monoclinic structure. Conventional (primitive) basis vectors are indicated in black (blue). The conventional unit cell is marked by solid black lines, while the primitive cell is dashed blue. (For interpretation of the colors in the figure(s), the reader is referred to the web version of this article.)

cell. In order to illustrate the use of these keywords, we work out the example of the C-centered monoclinic structure. Let the relation between the conventional basis vectors and the primitive ones used in the DFT calculation be the following, as illustrated in Fig. 1

$$\boldsymbol{c}_1 = \boldsymbol{a}_1 + \boldsymbol{a}_2,$$

 $\boldsymbol{c}_2 = -\boldsymbol{a}_1 + \boldsymbol{a}_2,$

 $c_3 = a_3$.

Also, assume that the two origins are related by the shift $0.3~a_3$. Then, the keywords refuc and shift UC should be used with arguments

```
-refUC=1,1,0,-1,1,0,0,0,1 -shiftUC=0,0,0.3
```

When IrRep is run without specifying the values for refUC and shiftUC, these parameters will be calculated automatically and printed together with vectors $\{a_1, a_2, a_3\}$ and $\{c_1, c_2, c_3\}$. When a basis transformation is applied, symmetry operations will be printed in both bases. For instance, the following lines illustrate the operations (only identity and inversion) printed by the code in the example of the C-centered crystal:

```
Space group C2/m (# 12) has 4 symmetry operations
### 1
: [ 0.0000
                      0.0000 0.0000]
translation
translation (refUC) : [ 0.0000
                      0.0000 0.0000]
axis: [0. 0. 1.]; angle = 0, inversion: False
### 2
: [ 0.0000
                          0.0000
                                 0.4000 1
translation
translation (refUC) : [ 0.0000
                          0.0000
                                 0.0000 ]
axis: [0. 1. 0.]; angle = 1 pi, inversion: False
```

Once keywords are provided, the class BandStructure reads the basic information from the output files of the DFT code, such as the plane-wave cutoff, number of bands, etc. In essence, the lattice vectors, positions of atoms and the energies and wavefunctions of electronic states are read in this way (see Sec. 3.3 for details). These parameters are found in the files listed in Table 2.

When the information is read, it is stored in an object of class BandStructure which is independent of the *ab initio* code used. Thus, if an interface to a new *ab initio* code is needed, one has to simply implement another constructor for the BandStructure class.

3.2. Determination of the space group

Next, basis vectors and atomic positions are passed to the library spglib [55], whose routine get_spacegroup gives the name and number of the space group, while get_symmetry returns the coset representatives of the space group's decomposition with respect to the translation group (see Sec. 2 for details). At this point, if the flag onlysym in Table 1 was set, IrRep prints the crystal structure and aforementioned coset representatives and then stops. Note that this utility can be useful for VASP even before running the DFT calculation to make sure that the configuration described in POSCAR really matches the assumed space group.

3.3. Reading wave functions

In VASP, Abinit and QE, eigenstates $|\Psi_{nk}\rangle$ of H(k) are expanded in a basis of plane waves $|k+G\rangle$:

$$\left|\Psi_{n\boldsymbol{k}}\right\rangle = \sum_{\boldsymbol{G}} C_{n\boldsymbol{k}}(\boldsymbol{G}) \left|\boldsymbol{k} + \boldsymbol{G}\right\rangle, \tag{7}$$

where the sum runs over all the reciprocal lattice vectors $\bf G$ whose energy is smaller than a cutoff, i.e. $\hbar^2({\bf k}+{\bf G})^2/2m_e < E_{\rm cut}$. The cutoff coincides with the value indicated by the user if Ecut in Table 1 was set; otherwise, it will be the cutoff used in the DFT calculation. After testing the code with different systems, we have noticed that usually a value $E_{\rm cut} \sim 50$ eV yields accurate results, since the most dominant coefficients in Eq. (7) correspond to short $\bf G$. After the application of the cutoff, the eigenstates $|\Psi_{n\bf k}\rangle$ are normalized.

If the DFT calculation ran with PAW pseudopotentials [56–58], the expansion Eq. (7) gives the smooth pseudo-wavefunctions $|\tilde{\Psi}_{nk}\rangle$, which are related to the all-electron wavefunctions $|\Psi_{nk}\rangle$ by a linear transformation $|\Psi_{nk}\rangle = T|\tilde{\Psi}_{nk}\rangle$. Note that $|\tilde{\Psi}_{nk}\rangle$ and $|\Psi_{nk}\rangle$ transform under symmetry operations in the same way. Hence for simplicity we work with the pseudo-wavefunctions.

In the Wannier90 input files (UNK*) the wavefunctions are written on a real-space grid. In that case we perform a fast-Fourier transform (FFT) to obtain the coefficients $C_{nk}(G)$ of Eq. (7).

3.4. Calculation of traces

For each k, symmetry operations g of its little group are picked one by one and expectation values $\langle \Psi_{nk} | g | \Psi_{nk} \rangle$ are calculated. Note that since the transformation properties of plane waves under translations are trivial, we need only iterate through the coset representatives g_i^k . The calculation of the traces depends on whether the DFT calculations were performed on scalar or spinor wavefunctions. Let us consider a $g = \{R \mid v\} \in G_k$ and show the calculation in both cases:

scalar wavefunctions

$$\langle \Psi_{n\boldsymbol{k}} | g | \Psi_{n\boldsymbol{k}} \rangle = \sum_{\boldsymbol{G}\boldsymbol{G}'} C_{n\boldsymbol{k}}^* (\boldsymbol{G}') C_{n\boldsymbol{k}} (\boldsymbol{G}) \langle \boldsymbol{k} + \boldsymbol{G}' | \{ R | \boldsymbol{v} \} | \boldsymbol{k} + \boldsymbol{G} \rangle.$$
(8)

From the transformation property of plane-waves,

$$g|\mathbf{k} + \mathbf{G}\rangle = e^{-i(R\mathbf{k} + R\mathbf{G}) \cdot \mathbf{v}} |R\mathbf{k} + R\mathbf{G}\rangle, \tag{9}$$

together with their orthogonality property,

$$\langle \mathbf{k}' + \mathbf{G}' | \mathbf{k} + \mathbf{G} \rangle = \delta_{\mathbf{G}', \mathbf{k} - \mathbf{k}' + \mathbf{G}}, \tag{10}$$

it follows that Eq. (8) is reduced to:

$$\langle \Psi_{n\mathbf{k}} | g | \Psi_{n\mathbf{k}} \rangle = \sum_{\mathbf{C}} C_{n\mathbf{k}}^* (R\mathbf{k} - \mathbf{k} + R\mathbf{G}) C_{n\mathbf{k}}(\mathbf{G}) e^{-i(R\mathbf{k} + R\mathbf{G}) \cdot \mathbf{v}}. \tag{11}$$

• for spinor wavefunctions $|\Psi_{n\mathbf{k}}\rangle = (|\Psi_{n\mathbf{k}}^{\uparrow}\rangle |\Psi_{n\mathbf{k}}^{\downarrow}\rangle)^T$ the matrix element reads:

$$\langle \Psi_{n\mathbf{k}} | g | \Psi_{n\mathbf{k}} \rangle = \sum_{\sigma \sigma'} S_{\sigma \sigma'}(g) \langle \Psi_{n\mathbf{k}}^{\sigma} | g | \Psi_{n\mathbf{k}}^{\sigma'} \rangle, \tag{12}$$

where brackets $<\Psi_{n\mathbf{k}}^{\sigma}|g|\Psi_{n\mathbf{k}}^{\sigma'}>$ are computed by means of Eq. (11) and S(g) is an SU(2) matrix corresponding to g.

After this calculation, IrRep adds the expectation values of degenerate eigenstates. Each of these sums is the trace $\chi(g)$ of a matrix K(g) belonging to the representation K defined in the subspace of degenerate eigenstates. These traces might be of interest by themselves, but can also be further used to identify the IRs.

3.5. Identification of irreducible representations

The characters χ_{α} of every IR K_{α} of G_k were obtained from the BCS [53] and are provided with the IrRep module. For each subspace of degenerate eigenstates, the magic formula (5) is applied, yielding the multiplicity m_{α}^{k} of IR K_{α} in the subspace of degenerate states. Notice that this procedure detects accidental degeneracies, which happen when eigenstates transforming under different IRs have the same energy.

At this point, the IR of each set of eigenstates is printed, together with the character of the IR. If traces of symmetry operations in the conventional cell differ from those in the cell used for the DFT calculation, they will be printed in both unit cells. Furthermore, IrRep also writes a file trace.txt, which can be passed directly to the program *CheckTopologicalMat* of BCS [44], in order to get information about (physical) elementary band representations and symmetry-based indicators [13,19–21] to diagnose the band topology.

By default, the procedure is performed for all the bands calculated by the DFT code. Nevertheless, the user can set values for IBstart and IBend in order to consider only bands in the range [IBstart,IBend]. This can be used to noticeably shorten the calculation time. Moreover, for the selected set of bands, the smallest direct and indirect gaps with respect to higher bands will be printed. For centrosymmetric crystals, the number of inversion-eigenvalue inversions (band inversions) and the \mathbb{Z}_2 index [6,59] will also be printed. In Sec. 4.1, we show an example of the output generated by IrRep where all these features are represented.

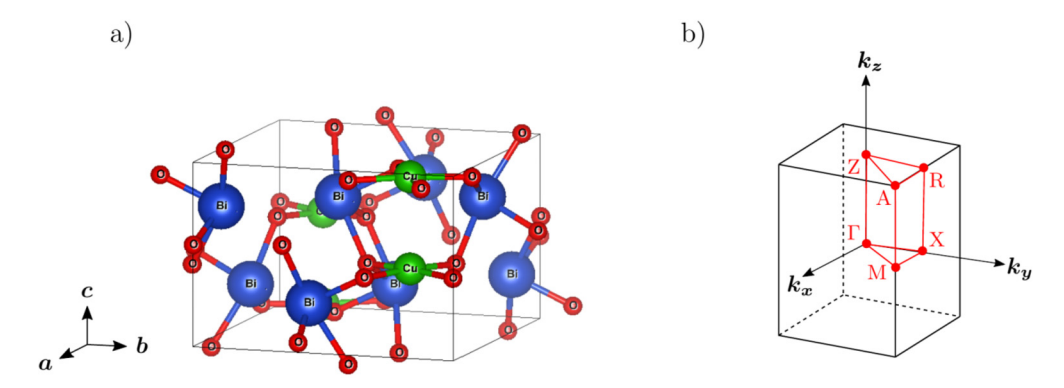


Fig. 2. Crystal structure of $CuBi_2O_4$. (a) Unit cell, with Cu, Bi and O atoms in green, blue and red, respectively. (b) BZ and irreducible BZ (red), with high-symmetry points. (For interpretation of the colors in the figure(s), the reader is referred to the web version of this article.)

3.6. Separation by symmetry eigenvalues

When writing the IRs, IrRep can separate the states by their eigenvalues with respect to a certain symmetry operation, if the index of that symmetry was given as isymsep (Table 1). Moreover, wave functions can be grouped by Kramers pairs, via the key groupKramers. The energies will also be written in a file, which can be used to plot bands. This data will be useful if the DFT calculation was done for an ordered set of k-points following a certain path in the BZ. Bands with different symmetry eigenvalues will be written in different files. The purpose of this feature is to respect the separation in the plot of bands, which is useful to study the role of symmetries in the protection of band crossings [45].

IrRep also contains routines to calculate the Zak phase and Wannier charge centers of a given set of bands (see keys ZAK and WCC in Table 1). Note that these functionalities work stably only for calculations employing norm-conserving pseudopotentials, and Ecut should not be specified in the command line (thus the DFT cutoff will be used). With the PAW method, due to the lack of consideration of the all-electron wavefunction, the results for symmetry separation and ZAK phase may be unreliable.

3.7. Writing the output

Finally, IrRep will return its output to the user. The output will be written in the CLI, from which it can be captured in plain text format. The output will also be printed in a JSON format file called irrep-output.json from which it can be easily parsed by downstream codes.

4. Example materials

In this section, we present the application of IrRep to two material examples, with different symmetries and topology, and analyzed by different DFT codes. With these examples, we cover the main functionalities of the code and also the subtlety related to the transformation between primitive and conventional basis. Input files to run the DFT calculations and input files that may be used to set IrRep's parameters for these examples can be found in the Github repository of the code [60].

4.1. Irreducible representations in CuBi₂O₄

First, we show the application of IrRep to $CuBi_2O_4$. In the paramagnetic phase, this material crystallizes in a tetragonal structure characterized by the non-symmorphic space group P4/ncc (No. 130) [61,62]. Its crystal structure and BZ are shown in Fig. 2.

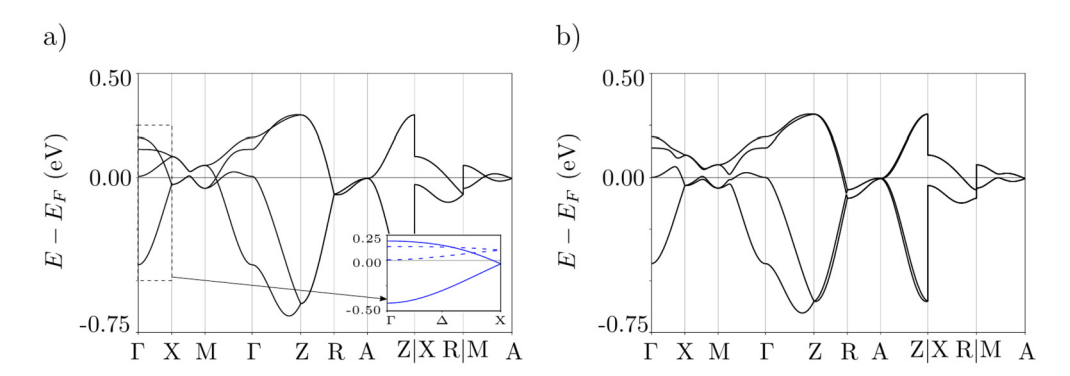


Fig. 3. Band structure of CuBi₂O₄ (a) without SOC included. Inset: bands in line Δ , connecting Γ to X, separated according to their eigenvalue of symmetry $\{m_x \mid 1/2, 0, 1/2\}$ in the little group; solid (dashed) corresponds to eigenvalue -1 (+1). (b) Band structure of CuBi₂O₄ with SOC included. (For interpretation of the colors in the figure(s), the reader is referred to the web version of this article.)

An interesting aspect of $CuBi_2O_4$ is found in reciprocal space: the little group of point A = (1/2, 1/2, 1/2), in the corner of the BZ, has only one (double-valued) IR with dimension 8. Its unusually large dimension makes it promising for the realization of high-degeneracy

Table 3IRs at high-symmetry points of the partially filled set of bands of CuBi₂O₄. In the second (third) row, IRs of the calculation without (with) SOC included are listed.

Γ	Х	M	Z	R	A
$\Gamma_4^+ \oplus \Gamma_2^+ \oplus \Gamma_4^- \oplus \Gamma_2^-$	$X_2 \oplus X_1$	$M_4 \oplus M_3$	2Z ₁	R_1R_2	A_3A_4
$2\overline{\Gamma}_6 \oplus 2\overline{\Gamma}_8$	$2\overline{X}_3\overline{X}_4$	$2\overline{M}_{5}$	$2\overline{Z}_5\overline{Z}_7$	$\overline{R}_4\overline{R}_4\oplus\overline{R}_3\overline{R}_3$	$\overline{A}_5\overline{A}_5$

unconventional fermions [63,64]. Also due to the fact that the number of electrons in the unit cell is not a multiple of 8, this IR forces $CuBi_2O_4$ to be a filling-enforced semimetal.

We have calculated the band structure of $CuBi_2O_4$ with Abinit, both treating spin trivially (scalar calculation) and including spin-orbit corrections (spinor calculation). A plane-wave cutoff of 500 eV and cold smearing [65] were used in the calculation. The BZ was sampled with a grid of $5 \times 5 \times 7$. Lattice parameters and atomic positions were taken from the Topological Quantum Chemistry database of materials [21]. The exchange-correlation term was approximated through General Gradient Approximation, in the Perdew Burke Ernzerhof [66] parametrization and PAW pseudopotentials were taken from Pseudo Dojo database [67]. Computed band structures can be seen in Fig. 3. Output files of IrRep are available in the examples folder of IrRep's official Github repository [60].

In the rest of the analysis, we focus on the partially-filled isolated set of bands cut by the Fermi level. IRs of the wave functions at high-symmetry points can be calculated by running the following lines (case with SOC):

IRs obtained in this way are written in Table 3. The following lines illustrate part of the output for the point R = (0, 1/2, 1/2). Even though the little group of R contains many coset representatives, only two of them (represented by indices 1 and 6) are shown here for brevity.

```
k-point
         5 : [0. 0.5 0.5]
 number of states = 8
   Energy
               degeneracy
                              irreps
                                        sym. operations
                                                1
                                                                6
                                         4.0000+0.0000j
                                                          0.0000+0.0006j
    7.1820
                              -R4(2.0)
    7.2232
                             -R3(2.0)
                                         4.0000+0.0000j -0.0000+0.0002j
inversion is # 9
number of inversions-odd Kramers pairs : 2
Gap with upper bands: 2.02
```

Interesting information about the bands and even about the chemistry of the system can be extracted from the knowledge of IRs. This set of IRs is consistent with an elementary band representation [13] induced from Wannier functions sitting in Wyckoff position 4c: $(B \uparrow G)_{4c}$ in the case without SOC, $({}^1E_2 {}^2E_2 \uparrow G)_{4c}$ with SOC, in the notation of Ref. [13]. According to the framework of band representations [68,69], which explains how bands in reciprocal space inherit their symmetry properties from orbitals in real space, the Wannier functions that induce these bands transform as a combination of $d_{x^2-y^2}$ and d_{xy} orbitals.

At every point k belonging to the line Δ that connects Γ to X, the little group contains the glide symmetry $g_X = \{m_X \mid 1/2, 0, 1/2\}$. This means that for $k \in \Delta$, wave functions of bands are also eigenstates of g_X , so that we can distinguish them by their eigenvalue under this symmetry. As we mentioned, IrRep can extract this eigenvalue, by running the option isymsep=14, which corresponds to g_X :

```
irrep -code=abinit -Ecut=100
    -fWFK=CuBi2O4-scalar_WFK -IBstart=145 -IBend=148
    -isymsep=14
```

The index corresponding to g_x can be derived beforehand by running the option onlysym. The result is shown in the inset of Fig. 3(a), where bands with eigenvalue -1 (+1) of g_x are indicated in solid (dashed). This calculation tells us that the crossings between dashed and solid bands are protected by g_x and thus cannot be gapped out without breaking this symmetry. Such criteria can be used to systematically study symmetry protected band crossings [45].

4.2. Bismuth: high order topological insulator

In this example, we will present the calculation of \mathbb{Z}_2 and \mathbb{Z}_4 indices with IrRep. For that, we will work with a particularly interesting and well-known material: bismuth.

In the presence of only time-reversal symmetry (TRS), an insulator can belong to either the trivial or the topological phase. The system cannot undergo a transition from one phase to the other if the gap is not closed or TRS is not broken in the process. In this spirit, the topology of the system can be characterized by a \mathbb{Z}_2 invariant [4,70,59], which is -1 (+1) in the topological (trivial) phase. With inversion, the \mathbb{Z}_2 invariant can be calculated by multiplying the inversion eigenvalues of Kramers pairs of occupied bands at all time-reversal invariant momenta (TRIM) [6]. In the topological case, we say that the system has a band-inversion.

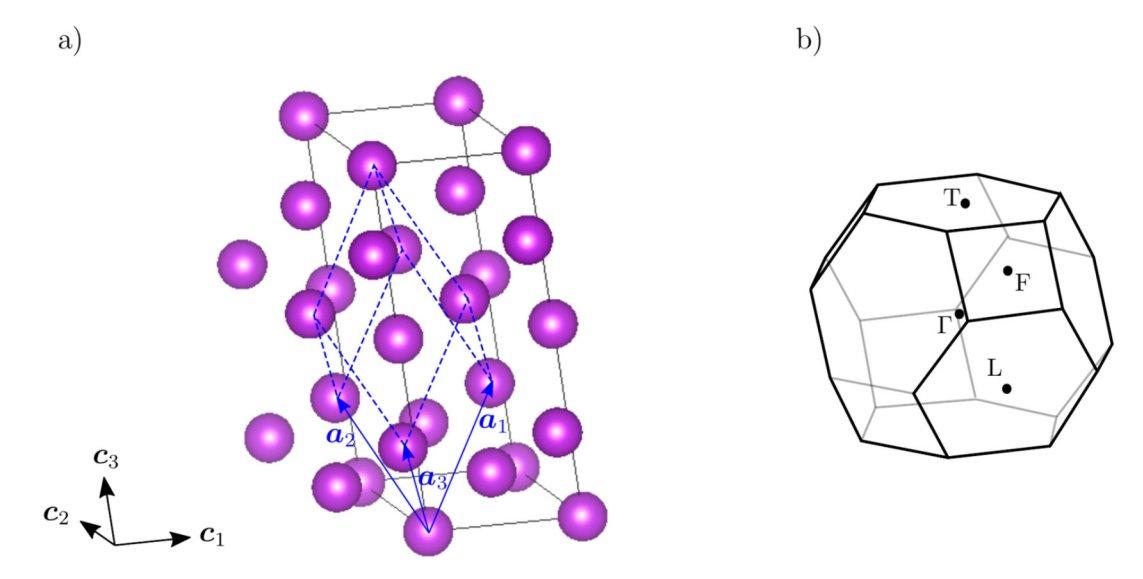


Fig. 4. a) Crystal structure of Bi in space group $R\overline{3}m$. Black lines delimit the conventional unit cell, whose basis vectors are $\{c_i\}_{i=1,2,3}$, while blue lines delimit the primitive unit cell used in the DFT calculation. b) Brillouin Zone corresponding to the primitive cell and TRIM (one from each star of k-points). (For interpretation of the colors in the figure(s), the reader is referred to the web version of this article.)

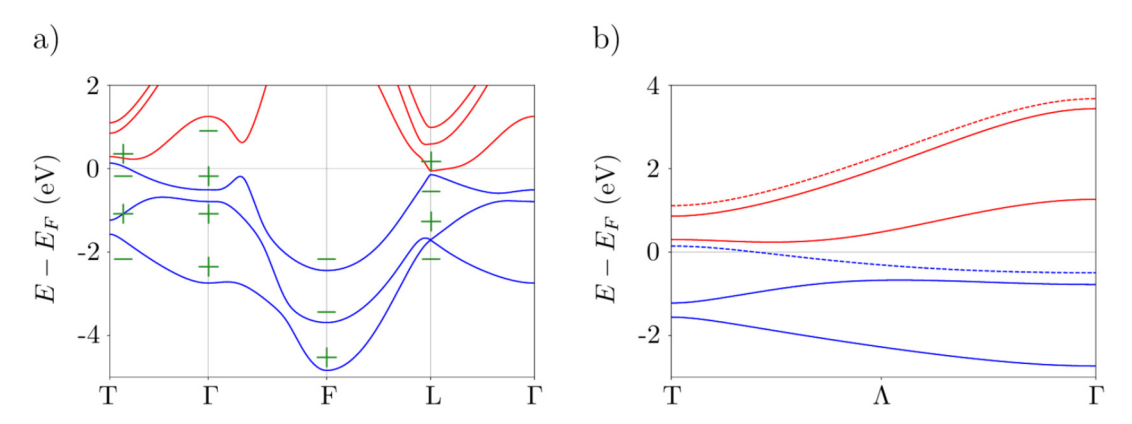


Fig. 5. Band structure of Bi in space group R3m. Since blue and red bands do not touch, we will ignore the electron-hole pockets and speak of occupied (blue) and unoccupied (red) bands. (a) Inversion eigenvalues at TRIM are indicated in green. (b) Bands along C_{3z} -invariant line Λ, which connects T to Γ; solid and dashed bands have C_{3z} eigenvalues -1 and $exp(\pm i\pi/3)$, respectively. (For interpretation of the colors in the figure(s), the reader is referred to the web version of this article.)

Crystal symmetries may enrich the topology of time-reversal invariant insulators, giving access to new phases, some of which can not be detected by the \mathbb{Z}_2 index. This is the case for bismuth in space group $R\overline{3}m$: the \mathbb{Z}_2 index has value +1, which means that the ground state corresponding to the occupied bands in Bi is a trivial insulator as per its \mathbb{Z}_2 index, according to the discussion above. However, in Ref. [27] it was shown that the ground state belongs to a higher-order topological phase, characterized by a \mathbb{Z}_4 index equal to 2. Here, we will reproduce with IrRep this analysis.

We have used VASP to perform *ab initio* calculations of Bi in the primitive unit cell. All calculations include spin-orbit corrections. A cutoff of 520 eV was set for the plane-wave basis, together with a Gaussian smearing. The BZ was sampled with a grid of $7 \times 7 \times 7$ k-points. We used PBE prescription as an approximation for the exchange-correlation term and PAW pseudopotentials [66]. The calculated bands are shown in Fig. 5(a). In Fig. 5(b), we show the bands separated by eigenvalues of C_{3z} using IrRep's option isymsep.

Space group $R\overline{3}m$ (No. 166) belongs to the rhombohedral family, in which conventional and primitive unit cells do not match, as can be seen in Fig. 4(a). Consequently, IrRep will need the transformation to the conventional cell. Even though we could let the code calculate refuc and shiftuc automatically, we will set them manually to illustrate them on a practical example. Since the origin of both, primitive and conventional cells is located in the same point, there is no need to specify shiftuc. Equation (6) takes the following form:

$$(\mathbf{c}_1, \mathbf{c}_2, \mathbf{c}_3)^T = \begin{pmatrix} 1 & -1 & 0 \\ 0 & 1 & -1 \\ 1 & 1 & 1 \end{pmatrix} (\mathbf{a}_1, \mathbf{a}_2, \mathbf{a}_3)^T,$$

so -refUC=1, -1, 0, 0, 1, -1, 1, 1, 1. In the following lines, which have been taken from the output of IrRep available among the examples in IrRep's Github repository [60], we show how IrRep prints the matrix of symmetry operations, in particular for the 3-fold rotation, in the settings before and after applying the transformation of the unit cell:

Table 4IRs at TRIM for the last 6 occupied bands in Bi, calculated with IrRep. In each k-point, IRs are written from left to right in ascending energy order, e.g., $\overline{T}_6\overline{T}_7$ is higher in energy than \overline{T}_8 .

T	Γ	F	L
$\overline{T}_9 \oplus \overline{T}_8 \oplus \overline{T}_6 \overline{T}_7$	$2\overline{\Gamma}_8\oplus\overline{\Gamma}_4\overline{\Gamma}_5$	$\overline{F}_3\overline{F}_4\oplus\overline{F}_5\overline{F}_6\oplus\overline{F}_5\overline{F}_6$	$\overline{L}_5\overline{L}_6\oplus\overline{L}_3\overline{L}_4\oplus\overline{L}_5\overline{L}_6$

2

```
rotation :
                  0
                      1 |
                                                      Ω
                              rotation :
                 0
                      0
                                (refUC)
                                                -1
                                                      0
             1
                                            1
spinor rot.
                     : | 0.500-0.866j
                                       -0.000-0.000j
                         0.000-0.000j
                                         0.500+0.866j
spinor rot. (refUC) :
                         0.500-0.866j
                                        -0.000-0.000j
                         0.000-0.000j
                                         0.500 + 0.866 j
translation
                     : [ 0.0000
                                   0.0000
                                            0.0000 1
translation (refUC) : [ 0.0000
                                   0.0000
                                            0.0000 1
axis: [0. 0. 1.]; angle = 2/3 pi, inversion: False
```

To make sure that the transformation is correct, one has to check whether matrices and translation vectors after the change of basis match with those in the table file of the corresponding space group. Alternatively, they can be compared to matrices and translations in the GENPOS application of the BCS [71]. The next step is to calculate the IRs of occupied bands (Table 4). For that, we call IrRep with the keywords written in the following lines:

With the knowledge of the IRs and their inversion eigenvalues [see Fig. 5(a)], we conclude that the total number of (Kramers pairs of) -1 inversion eigenvalues in the occupied bands is even, thus the \mathbb{Z}_2 index $z_2=+1$. However, there are two band inversions between Γ and Γ that the \mathbb{Z}_2 invariant cannot detect. Indeed, this double band inversion leads to the \mathbb{Z}_4 invariant $z_4=2$, since the number of Kramers pairs of -1 inversion eigenvalues is equal to 2 mod 4. This means that Bi is a higher-order topological insulator (HOTI) [27]. The value of the \mathbb{Z}_4 index and number of -1 inversion eigenvalues are, by default, calculated and printed by IrRep; in the following lines, we show the way in which they are printed by the code, together with information about the direct and general gaps¹:

```
Number of inversions-odd Kramers pairs IN THE LISTED KPOINTS : 6 Z4= 2 Minimal direct gap : 0.08857033154551353 eV Indirect gap : -0.1886089499035215 eV
```

5. Conclusion

IrRep is a Python code for the calculation of irreducible representations of DFT calculated bands at high-symmetry points. It is a powerful tool for the detection and classification of topological sets of bands and materials, applicable with calculations performed both with or without SOC and using unit cells that might be non-conventional. Its structure keeps the implementation of interfaces to planewave DFT codes simple; currently, it is compatible with VASP, Abinit, Quantum Espresso and any code that has an interface to Wannier90 (which covers most of the popular DFT codes). Additionally, routines for separating bands based on an eigenvalue of certain symmetry operation are included. IrRep can be freely downloaded from https://github.com/stepan-tsirkin/irrep and/or installed with pip and its official webpage can be found in https://irrep.dipc.org/; the repository also contains examples, including the analysis of CuBi₂O₄ that we have presented in this work to illustrate the utility of the code.

Software availability

All software used and developed in this article (except VASP) is open-source and available for free. ITRep is available via pip [72] and GitHub [60]. It also has an official webpage [73]. External libraries used in ITRep include spglib [55], NumPy [74], SciPy [75], lazy-property [76], Click [77], monty [78] and ruamel.yaml [79]. VASP is commercial software available from the developers for a fee [80]. Other codes are available at [81] (Wannier90), [82] (QuantumEspresso) and [83] (Abinit). Figures of crystal structures were generated with VESTA [84]. Band structures were plotted with BEplot [85], which uses Matplotlib [86]. Inkscape vector graphics editor [87] was used in most figures.

¹ Here the gap refers only to the high-symmetry points included in the calculation. The real gap may be smaller (and even may close) at some arbitrary point away from high-symmetry points.

Declaration of competing interest

The authors declare that they have no known competing financial interests or personal relationships that could have appeared to influence the work reported in this paper.

Acknowledgements

M.G.V. and M.I. acknowledges the Spanish Ministerio de Ciencia e Innovación (grant number PID2019-109905GB-C21) and DFG IN-CIEN2019-000356 from Gipuzkoako Foru Aldundia. B. B. acknowledges the support of the Alfred P. Sloan Foundation, and the National Science Foundation under grant DMR-1945058. The work of J.L.M. has been supported by Spanish Science Ministry grant PGC2018-094626-BC21 (MCIU/AEI/FEDER, EU) and Basque Government grant IT979-16. MKH acknowledges support by the U.S. Department of Energy, Office of Science, Office of Basic Energy Sciences, Materials Sciences and Engineering Division under Contract No. DE-AC02-05-CH11231 (Materials Project program KC23MP). S.S.T. and T.N. acknowledge support from NCCR MARVEL and from the European Union's Horizon 2020 research and innovation program (ERC-StG-Neupert-757867PARATOP). S.S.T. also acknowledges support from the Swiss National Science Foundation (grant number: PP00P2 176877).

References

- [1] H. Weyl, The Theory of Groups and Quantum Mechanics, Courier Corporation, 1950.
- [2] L.P. Bouckaert, R. Smoluchowski, E. Wigner, Phys. Rev. 50 (1) (1936) 58.
- [3] C. Bradley, A. Cracknell, The Mathematical Theory of Symmetry in Solids: Representation Theory for Point Groups and Space Groups, Clarendon Press, Oxford, 2010.
- [4] C.L. Kane, E.J. Mele, Phys. Rev. Lett. 95 (2005) 226801, https://doi.org/10.1103/PhysRevLett.95.226801, https://link.aps.org/doi/10.1103/PhysRevLett.95.226801.
- [5] B.A. Bernevig, S.-C. Zhang, Phys. Rev. Lett. 96 (2006) 106802, https://doi.org/10.1103/PhysRevLett.96.106802, https://link.aps.org/doi/10.1103/PhysRevLett.96.106802.
- [6] L. Fu, C.L. Kane, Phys. Rev. B 76 (2007) 045302, https://doi.org/10.1103/PhysRevB.76.045302, https://link.aps.org/doi/10.1103/PhysRevB.76.045302.
- [7] J.C.Y. Teo, L. Fu, C.L. Kane, Phys. Rev. B 78 (2008) 045426, https://doi.org/10.1103/PhysRevB.78.045426, https://link.aps.org/doi/10.1103/PhysRevB.78.045426.
- [8] A.M. Turner, Y. Zhang, A. Vishwanath, Phys. Rev. B 82 (2010) 241102, https://doi.org/10.1103/PhysRevB.82, https://link.aps.org/doi/10.1103/PhysRevB.82.241102.
- [9] T.L. Hughes, E. Prodan, B.A. Bernevig, Phys. Rev. B 83 (2011) 245132, https://doi.org/10.1103/PhysRevB.83.245132, https://link.aps.org/doi/10.1103/PhysRevB.83.245132.
- [10] L. Fu, Phys. Rev. Lett. 106 (2011) 106802, https://doi.org/10.1103/PhysRevLett.106.106802, https://link.aps.org/doi/10.1103/PhysRevLett.106.106802.
- [11] T.H. Hsieh, H. Lin, J. Liu, W. Duan, A. Bansil, L. Fu, Nat. Commun. 3 (2012) 932.
- [12] A.M. Turner, Y. Zhang, R.S.K. Mong, A. Vishwanath, Phys. Rev. B 85 (2012) 165120, https://doi.org/10.1103/PhysRevB.85.165120, https://link.aps.org/doi/10.1103/PhysRevB.85.165120.
- [13] B. Bradlyn, L. Elcoro, J. Cano, M.G. Vergniory, Z. Wang, C. Felser, M.I. Aroyo, B.A. Bernevig, Nature 547 (7663) (2017) 298-305, https://doi.org/10.1038/nature23268.
- [14] B. Bradlyn, L. Elcoro, M.G. Vergniory, J. Cano, Z. Wang, C. Felser, M.I. Aroyo, B.A. Bernevig, Phys. Rev. B 97 (2018) 035138, https://doi.org/10.1103/PhysRevB.97.035138, https://link.aps.org/doi/10.1103/PhysRevB.97.035138.
- [15] M.G. Vergniory, L. Elcoro, Z. Wang, J. Cano, C. Felser, M.I. Aroyo, B.A. Bernevig, B. Bradlyn, Phys. Rev. E 96 (2017) 023310, https://doi.org/10.1103/PhysRevE.96.023310, https://link.aps.org/doi/10.1103/PhysRevE.96.023310.
- [16] J. Cano, B. Bradlyn, Band representations and topological quantum chemistry, arXiv preprint, arXiv:2006.04890, 2020.
- [17] H.C. Po, J. Phys. Condens. Matter 32 (26) (2020) 263001.
- [18] L. Elcoro, Z. Song, B.A. Bernevig, Application of the induction procedure and the Smith decomposition in the calculation and topological classification of electronic band structures in the 230 space groups, arXiv preprint, arXiv:2002.03836, 2020.
- [19] Z. Song, T. Zhang, Z. Fang, C. Fang, Nat. Commun. 9 (1) (2018) 3530, https://doi.org/10.1038/s41467-018-06010-w.
- [20] H.C. Po, A. Vishwanath, H. Watanabe, Nat. Commun. 8 (1) (2017) 50, https://doi.org/10.1038/s41467-017-00133-2.
- [21] M.G. Vergniory, L. Elcoro, C. Felser, N. Regnault, B.A. Bernevig, Z. Wang, Nature 566 (7745) (2019) 480-485, https://doi.org/10.1038/s41586-019-0954-4.
- [22] T. Zhang, Y. Jiang, Z. Song, H. Huang, Y. He, Z. Fang, H. Weng, C. Fang, Nature 566 (7745) (2019) 475-479, https://doi.org/10.1038/s41586-019-0944-6.
- [23] F. Tang, H.C. Po, A. Vishwanath, X. Wan, Nat. Phys. 15 (5) (2019) 470-476, https://doi.org/10.1038/s41567-019-0418-7.
- [24] Y. Xu, L. Elcoro, Z. Song, B.J. Wieder, M. Vergniory, N. Regnault, Y. Chen, C. Felser, B.A. Bernevig, G. Sharma, et al., High-throughput calculations of antiferromagnetic topological materials from magnetic topological quantum chemistry, arXiv preprint, arXiv:2003.00012, 2020.
- [25] H.C. Po, H. Watanabe, A. Vishwanath, Fragile topology and Wannier obstructions, arXiv preprint, arXiv:1709.06551, 2017.
- [26] F. Schindler, A.M. Cook, M.G. Vergniory, Z. Wang, S.S.P. Parkin, B.A. Bernevig, T. Neupert, Sci. Adv. 4 (6) (2018), https://doi.org/10.1126/sciadv.aat0346, https://advances.sciencemag.org/content/4/6/eaat0346.
- [27] F. Schindler, Z. Wang, M.G. Vergniory, A.M. Cook, A. Murani, S. Sengupta, A.Y. Kasumov, R. Deblock, S. Jeon, I. Drozdov, H. Bouchiat, S. Guéron, A. Yazdani, B.A. Bernevig, T. Neupert, Nat. Phys. 14 (2018) 918, https://doi.org/10.1038/s41567-018-0224-7.
- [28] F. Schindler, M. Brzezińska, W.A. Benalcazar, M. Iraola, A. Bouhon, S.S. Tsirkin, M.G. Vergniory, T. Neupert, Phys. Rev. Res. 1 (2019) 033074, https://doi.org/10.1103/PhysRevResearch.1.033074, https://link.aps.org/doi/10.1103/PhysRevResearch.1.033074.
- [29] M.B. de Paz, M.G. Vergniory, D. Bercioux, A. García-Etxarri, B. Bradlyn, Phys. Rev. Res. 1 (2019) 032005, https://doi.org/10.1103/PhysRevResearch.1.032005, https://doi.org/10.1103/PhysRevResearch.1.032005
- [30] B. Bradlyn, Z. Wang, J. Cano, B.A. Bernevig, Phys. Rev. B 99 (2019) 045140, https://doi.org/10.1103/PhysRevB.99.045140, https://link.aps.org/doi/10.1103/PhysRevB.99.
- [31] B.J. Wieder, B.A. Bernevig, The axion insulator as a pump of fragile topology, arXiv preprint, arXiv:1810.02373, 2018.
- [32] B.J. Wieder, Z. Wang, J. Cano, X. Dai, L.M. Schoop, B. Bradlyn, B.A. Bernevig, Nat. Commun. 11 (1) (2020) 1-13.
- [33] W. Shi, B.J. Wieder, H. Meyerheim, Y. Sun, Y. Zhang, Y. Li, L. Shen, Y. Qi, L. Yang, J. Jena, et al., A charge-density-wave Weyl semimetal, arXiv preprint, arXiv:1909.04037, 2019.
- [34] J. Gooth, B. Bradlyn, S. Honnali, C. Schindler, N. Kumar, J. Noky, Y. Qi, C. Shekhar, Y. Sun, Z. Wang, B.A. Bernevig, C. Felser, Nature 575 (7782) (2019) 315–319, https://doi.org/10.1038/s41586-019-1630-4.
- [35] Z. Wang, B.J. Wieder, J. Li, B. Yan, B.A. Bernevig, Phys. Rev. Lett. 123 (18) (2019) 186401.
- [36] G. Kresse, J. Furthmüller, Phys. Rev. B 54 (1996) 11169–11186, https://doi.org/10.1103/PhysRevB.54.11169, https://link.aps.org/doi/10.1103/PhysRevB.54.11169.
- [37] X. Gonze, F. Jollet, F. Abreu Araujo, D. Adams, B. Amadon, T. Applencourt, C. Audouze, J.-M. Beuken, J. Bieder, A. Bokhanchuk, E. Bousquet, F. Bruneval, D. Caliste, M. Côté, F. Dahm, F. Da Pieve, M. Delaveau, M. Di Gennaro, B. Dorado, C. Espejo, G. Geneste, L. Genovese, A. Gerossier, M. Giantomassi, Y. Gillet, D. Hamann, L. He, G. Jomard, J. Laflamme Janssen, S. Le Roux, A. Levitt, A. Lherbier, F. Liu, I. Lukačević, A. Martin, C. Martins, M. Oliveira, S. Poncé, Y. Pouillon, T. Rangel, G.M. Rignanese, A. Romero, B. Rousseau, O. Rubel, A. Shukri, M. Stankovski, M. Torrent, M. Van Setten, B. Van Troeye, M. Verstraete, D. Waroquiers, J. Wiktor, B. Xu, A. Zhou, J. Zwanziger, Comput. Phys. Commun. 205 (2016) 106–131, https://doi.org/10.1016/j.cpc.2016.04.003.
- [38] P. Giannozzi, S. Baroni, N. Bonini, M. Calandra, R. Car, C. Cavazzoni, D. Ceresoli, G.L. Chiarotti, M. Cococcioni, I. Dabo, A.D. Corso, S. de Gironcoli, S. Fabris, G. Fratesi, R. Gebauer, U. Gerstmann, C. Gougoussis, A. Kokalj, M. Lazzeri, L. Martin-Samos, N. Marzari, F. Mauri, R. Mazzarello, S. Paolini, A. Pasquarello, L. Paulatto, C. Sbraccia, S. Scandolo, G. Sclauzero, A.P. Seitsonen, A. Smogunov, P. Umari, R.M. Wentzcovitch, J. Phys. Condens. Matter 21 (39) (2009) 395502, https://doi.org/10.1088/0953-8984/21/39/395502.

- [39] G. Pizzi, V. Vitale, R. Arita, S. Blügel, F. Freimuth, G. Géranton, M. Gibertini, D. Gresch, C. Johnson, T. Koretsune, J. Ibañez-Azpiroz, H. Lee, J.-M. Lihm, D. Marchand, A. Marrazzo, Y. Mokrousov, J.I. Mustafa, Y. Nohara, Y. Nomura, L. Paulatto, S. Poncé, T. Ponweiser, J. Qiao, F. Thöle, S.S. Tsirkin, M. Wierzbowska, N. Marzari, D. Vanderbilt, I. Souza, A.A. Mostofi, J.R. Yates, J. Phys. Condens. Matter 32 (16) (2020) 165902, https://doi.org/10.1088/1361-648x/ab51ff.
- [40] J.M. Soler, E. Artacho, J.D. Gale, A. García, J. Junquera, P. Ordejón, D. SánchezPortal, J. Phys. Condens. Matter 14 (11) (2002) 2745–2779, https://doi.org/10.1088/0953-8984/14/11/302.
- [41] J. Gao, Q. Wu, C. Persson, Z. Wang, Irvsp: to obtain irreducible representations of electronic states in the VASP, arXiv:2002.04032, 2020.
- [42] Topological materials database, https://topologicalquantumchemistry.org, 2019.
- [43] A. Matsugatani, S. Ono, Y. Nomura, H. Watanabe, qeirreps: An open-source program for Quantum ESPRESSO to compute irreducible representations of Bloch wavefunctions. arXiv preprint. arXiv:2006.00194, 2020.
- [44] Bilbao Crystallographic Server, https://www.cryst.ehu.es/.
- [45] S.S. Tsirkin, I. Souza, D. Vanderbilt, Phys. Rev. B 96 (2017) 045102, https://doi.org/10.1103/PhysRevB.96.045102, https://link.aps.org/doi/10.1103/PhysRevB.96.045102.
- [46] J.F. Khoury, A.J.E. Rettie, M.A. Khan, N.J. Ghimire, I.n. Robredo, J.E. Pfluger, K. Pal, C. Wolverton, A. Bergara, J.S. Jiang, L.M. Schoop, M.G. Vergniory, J.F. Mitchell, D.Y. Chung, M.G. Kanatzidis, J. Am. Chem. Soc. 141 (48) (2019) 19130–19137, https://doi.org/10.1021/jacs.9b10147, pMID: 31697089.
- [47] J.F. Khoury, A.J.E. Rettie, I. n. Robredo, M.J. Krogstad, C.D. Malliakas, A. Bergara, M.G. Vergniory, R. Osborn, S. Rosenkranz, D.Y. Chung, M.G. Kanatzidis, J. Am. Chem. Soc. 142 (13) (2020) 6312–6323, https://doi.org/10.1021/jacs.0c00809, pMID: 32160464.
- [48] I. Robredo, M.G. Vergniory, B. Bradlyn, Phys. Rev. Mater. 3 (2019) 041202, https://doi.org/10.1103/PhysRevMaterials.3.041202, https://link.aps.org/doi/10.1103/PhysRevMaterials.3.041202.
- [49] M.-Á. Sánchez-Martínez, I. Robredo, A. Bidaurrazaga, A. Bergara, F. de Juan, A.G. Grushin, M.G. Vergniory, J. Phys. Mater. 3 (1) (2019) 014001, https://doi.org/10.1088/2515-7639/ab3ea2.
- [50] J. Ibañez-Azpiroz, F. de Juan, I. Souza, Quantitative analysis of two-band k · p models describing the shift-current photoconductivity, arXiv:1910.06172, 2019.
- [51] J. Ibañez Azpiroz, I. Souza, F. de Juan, Phys. Rev. Res. 2 (2020) 013263, https://doi.org/10.1103/PhysRevResearch.2.013263, https://link.aps.org/doi/10.1103/PhysRevResearch.2.013263.
- [52] M.I. Aroyo (Ed.), International Tables for Crystallography, Vol. A, International Union of Crystallography, 2016, https://doi.org/10.1107/97809553602060000114, http://it.iucr.org/A/.
- [53] L. Elcoro, B. Bradlyn, Z. Wang, M.G. Vergniory, J. Cano, C. Felser, B.A. Bernevig, D. Orobengoa, G. de la Flor, M.I. Aroyo, J. Appl. Crystallogr. 50 (5) (2017) 1457–1477, https://doi.org/10.1107/S1600576717011712.
- [54] J.P. Serre, Linear Representations of Finite Groups, Springer, 1996.
- [55] A. Togo, I. Tanaka, Spglib: a software library for crystal symmetry search, arXiv:1808.01590, 2018.
- [56] P.E. Blöchl, Phys. Rev. B 50 (1994) 17953-17979, https://doi.org/10.1103/PhysRevB.50.17953, https://link.aps.org/doi/10.1103/PhysRevB.50.17953.
- [57] G. Kresse, D. Joubert, Phys. Rev. B 59 (1999) 1758-1775, https://doi.org/10.1103/PhysRevB.59.1758, https://link.aps.org/doi/10.1103/PhysRevB.59.1758.
- [58] M. Torrent, F. Jollet, F. Bottin, G. Zérah, X. Gonze, Comput. Mater. Sci. 42 (2) (2008) 337–351, https://doi.org/10.1016/j.commatsci.2007.07.020.
- [59] J.E. Moore, L. Balents, Phys. Rev. B 75 (2007) 121306, https://doi.org/10.1103/PhysRevB.75.121306, https://link.aps.org/doi/10.1103/PhysRevB.75.121306.
- [60] Official repository of Irrep, https://github.com/stepan-tsirkin/irrep.
- [61] K. Yamada, K.-i. Takada, S. Hosoya, Y. Watanabe, Y. Endoh, N. Tomonaga, T. Suzuki, T. Ishigaki, T. Kamiyama, H. Asano, F. Izumi, J. Phys. Soc. Jpn. 60 (7) (1991) 2406–2414, https://doi.org/10.1143/JPSI.60.2406.
- [62] D. Thomas, J.-C. Boivin, J. Tréhoux, Bull. Soc. Fr. Minéral. Cristallogr. 99 (4) (1976) 193–196, https://doi.org/10.3406/bulmi.1976.7065, https://www.persee.fr/doc/bulmi_0037-9328_1976_num_99_4_7065.
- [63] B. Bradlyn, J. Cano, Z. Wang, M.G. Vergniory, C. Felser, R.J. Cava, B.A. Bernevig, Science 353 (6299) (2016), https://doi.org/10.1126/science.aaf5037, https://science.sciencemag.org/content/353/6299/aaf5037.
- [64] B.I. Wieder, Y. Kim, A. Rappe, C. Kane, Phys. Rev. Lett. 116 (18) (2016) 186402.
- [65] N. Marzari, Ab-initio molecular dynamics for metallic systems, PhD Thesis http://theossrv1.epfl.ch/Main/Theses?action=download&upname=Marzari_thesis_1996.pdf,
- [66] J.P. Perdew, K. Burke, M. Ernzerhof, Phys. Rev. Lett. 77 (1996) 3865–3868, https://doi.org/10.1103/PhysRevLett.77.3865, https://link.aps.org/doi/10.1103/PhysRevLett.77.3865, https://doi.org/10.1103/PhysRevLett.77.3865.
- [67] database Pseudo, Dojo database of pseudopotentials, http://www.pseudo-dojo.org/index.html.
- [68] J. Zak, Phys. Rev. Lett. 45 (1980) 1025-1028, https://doi.org/10.1103/PhysRevLett.45.1025, https://link.aps.org/doi/10.1103/PhysRevLett.45.1025.
- [69] J. Zak. Phys. Rev. B 23 (1981) 2824–2835. https://doi.org/10.1103/PhysRevB.23.2824. https://link.aps.org/doi/10.1103/PhysRevB.23.2824.
- [70] C.L. Kane, E.J. Mele, Phys. Rev. Lett. 95 (14) (2005) 146802.
- [71] M.I. Aroyo, J.M. Perez-Mato, C. Capillas, E. Kroumova, S. Ivantchev, G. Madariaga, A. Kirov, H. Wondratschek, Z. Kristallogr. 221 (1) (2006) 15–27, https://doi.org/10.1524/zkri.2006.221.1.15, https://www.degruyter.com/view/journals/zkri/221/1/article-p15.xml.
- [72] PyPI repository, https://pypi.org/project/irrep.
- [73] Official webpage of Irrep, http://irrep.dipc.org/.
- [74] T.E. Oliphant, A Guide to NumPy, Vol. 1, Trelgol Publishing USA, 2006.
- [75] P. Virtanen, R. Gommers, T.E. Oliphant, M. Haberland, T. Reddy, D. Cournapeau, E. Burovski, P. Peterson, W. Weckesser, J. Bright, S.J. van der Walt, M. Brett, J. Wilson, K. Jarrod Millman, N. Mayorov, A.R.J. Nelson, E. Jones, R. Kern, E. Larson, C. Carey, İ. Polat, Y. Feng, E.W. Moore, J. VanderPlas, D. Laxalde, J. Perktold, R. Cimrman, I. Henriksen, E.A. Quintero, C.R. Harris, A.M. Archibald, A.H. Ribeiro, F. Pedregosa, P. van Mulbregt, S.. Contributors, Nat. Methods (2020), https://doi.org/10.1038/s41592-019-0686-2.
- [76] lazy-property python module, https://pypi.org/project/lazy-property.
- [77] Click python package, https://click.palletsprojects.com/en/8.0.x/.
- [78] Monty Python module, https://pypi.org/project/monty/.
- [79] ruamel.yaml python module, https://pypi.org/project/ruamel.yaml/.
- [80] VASP code, https://www.vasp.at/.
- [81] Wannier90 code, http://www.wannier.org/.
- [82] QuantumEspresso code, https://www.quantum-espresso.org/.
- [83] Abinit code, https://www.abinit.org/.
- [84] K. Momma, F. Izumi, J. Appl. Crystallogr. 44 (6) (2011) 1272–1276, https://doi.org/10.1107/S0021889811038970.
- [85] Repository of BEplot, https://gitlab.com/MIraola/BEplot.
- [86] J.D. Hunter, Comput. Sci. Eng. 9 (3) (2007) 90-95, https://doi.org/10.1109/MCSE.2007.55.
- [87] Inkscape vector graphics editor, https://inkscape.org.